applied sciences

MDPI

Article

A Nonlinear Robust Sliding Mode Controller with Auxiliary Dynamic System for the Hovering Flight of a Tilt Tri-Rotor UAV

Guang He *, Li Yu, Huaping Huang and Xiangke Wang

College of Intelligence Science and Technology, National University of Defense Technology, Changsha 410073, China; yulisdu@163.com (L.Y.); huanghuaping14@nudt.edu.cn (H.H.); xkwang@nudt.edu.cn (X.W.)

* Correspondence: heguang@nudt.edu.cn; Tel.: +86-0731-8457-6037-804

Received: 18 August 2020; Accepted: 14 September 2020; Published: 19 September 2020

Abstract: The tilt tri-rotor unmanned aerial vehicle (UAV) has three flight modes: the hover mode, the transition mode, and the fixed-wing mode. Controller design in the hover mode is the premise of realizing stable flight of this kind of UAV. Due to the particular structure with odd rotors and strong nonlinearity, the modeling and control of the tilt tri-rotor UAV remain an active and ongoing research topic. To overcome these problems and achieve stable flight control, this paper proposes a sliding mode-based nonlinear control scheme for the hovering flight of a tilt tri-rotor UAV, consisting of position control, attitude control, and control allocation. First, the mathematical model of the UAV is given by using the Newton–Euler formulation. Second, a cascade flight controller consisting of the position controller and the attitude controller is developed based on sliding mode control (SMC). For the position controller, an auxiliary dynamic system composed of the hyperbolic tangent functions is introduced to the SMC approach for constraining the output magnitude of the thrust and the reference attitudes. Besides, a disturbance observer is applied to the attitude controller to alleviate the chattering and improve robustness. Furthermore, according to the structural characteristics of the tilt tri-rotor UAV, a control allocation algorithm is developed to map the virtual control quantities calculated by the cascade flight controller to the actual actuators. Simulations are conducted to verify the robustness against the external disturbances and parameter variations, and the performance comparisons with two other control schemes are also given. Finally, the experiment is also carried out to validate the performance of the proposed control scheme.

Keywords: hovering flight control; control allocation; sliding mode control; auxiliary dynamic

1. Introduction

The tilt-rotor UAV (TRUAV) can take-off and land vertically, and also has the advantage of long endurance, which has drawn considerable interest from interested military and civilian parties due to its potential applications. According to the rotor number, the tilt-rotor UAV can be divided into two types: Dual-TRUAV and Multi-TRUAV [1]. The Engle eye UAV, which has two tilt rotors mounted on the wingtip, is the representative and first practical application of the Dual-TRUAV [2]. Adopting the same configuration, Korea Aerospace Research Institute (KARI) and Korean Air (KA) have developed a tilt-rotor UAV named Smart UAV [3,4]. The flight tests of Smart UAV are completed, but until now, this type of UAV has not been applied in practice. The Dual-TRUAV has the disadvantages of a complex tilt mechanism and serious interference between the rotors and wings, which means that its design, manufacturing, and flight control have great technical challenges and high cost. In view of that, many countries have begun to explore and research the Multi-TRUAVs, which provides a

new solution for the development and application of the tilt rotor UAVs, such as the Panther of Israel Aircraft Industries [5], TURAC of Istanbul University [6], etc.

The Multi-TRUAVs have a simplified mechanical structure and more symmetrical aircraft layout in the longitudinal direction. However, due to the increase of the rotors and the existence of multiple flight modes, there are still some problems that need to be solved in the design and flight control of Multi-TRUAVs, thus it has attracted the attention of many researchers [5–15]. Ozdemir designs a flying-wing UAV named TURAC which has two rotors and one main coaxial fan [8]. The mathematical model of TURAC was derived and the aerodynamic coefficients were calculated by CFD simulations. Based on these, the transition strategy was also proposed to achieve mode switching [9]. Papachristos designed a tilt tri-rotor UAV, all of whose rotors can tilt. Based on this prototype, a series of research work was carried out [10,11]. It adopted an explicit model predictive control scheme relying on constrained multiparametric optimization to achieve flight control. Chen developed a quad tilt-rotor UAV; only the two front rotors can tilt. The model of the vehicle is constructed based on experiments and numerical analysis, and a control scheme composed of robust servo linear quadratic regulator and extended state observer is designed [12]. Carlson and Chowdhury developed a unique tilt-rotor UAV which was controlled by a proportional integral differential (PID) controller; the simulation and flight test were also carried out [13,14]. As for a tilt tri-rotor UAV with the rear servo's stuck fault, Xian designed a robust integral of the signum of the error based controller to maintain the tilt tri-rotor UAV's attitude stability [15].

In the actual flight process of the Multi-TRUAVs, it commonly suffers from many control difficulties. A PID control method commonly was used in the flight control of the tilt rotor UAVs [16,17]. Yunus adopted the conventional PID control to generate the control inputs of a tilt rotor quadplane, and the control performances of the tilt-rotor configuration and the pusher quadplane configuration were also compared. The simulation results indicated that the conventional PID control is still more challenging in the control of the tilt-rotor configuration [17]. Liu reviewed some linear control methods such as state feedback, LQR, and robust control which were often used in the controller design of the tilt rotor UAVs [1]. However, these methods struggle to deal with the strong nonlinearity and external disturbances. The dynamic characteristics of the tilt rotor UAVs are inherently strong nonlinear. Meanwhile, the model is usually subject to parametric uncertainties and unmodeled dynamics. Therefore, for the Multi-TRUAVs, the advanced nonlinear control schemes are required to achieve good robust performance in autonomous flight with respect to external disturbances, parametric uncertainties, unmodeled dynamics, etc. [18].

In view of strong nonlinear characteristics of the tilt rotor UAVs, nonlinear dynamic inversion method and backstepping method are applied to the flight control design. Francesco designed an attitude controller based on incremental nonlinear dynamic inversion technology for a tilted quadrotor UAV with a central duct [19]. Kong designed a tilting quadrotor UAV and proposed a nonlinear controller based on backstepping [20]. Based on the proposed controller, the flight test of the hover mode and simulation analysis of the transition mode were completed. These two methods require an accurate mathematical model of the controlled object. However, for the tilt rotor UAVs, the precise modeling is very difficult, which limits the application of these two methods. To attenuate the influence of parametric uncertainties and external disturbances, many efforts have been devoted to designing a robust controller for the tilt-rotor UAVs. Yildiz designed an adaptive nonlinear hierarchical controller for a quad tilt-wing UAV [21]. Uncertainties in the aircraft dynamics can be handled with the designed control scheme. However, the adaptive law was not designed with a projection algorithm, so that the estimated parameters may not be bounded. Papachristos proposed an explicit model predictive control scheme relying on multiparameter constrained optimization for a Y-type aircraft with tiltable rotors [10,22]. At present, model predictive control requires high airborne computing resources and is more suitable for the controlled objects with slow dynamics.

As an effective method in dealing with nonlinear systems with model uncertainties, the sliding mode control (SMC) has also been used for flight control. Yoo proposed the fuzzy sliding mode control

scheme for a tilt-rotor UAV with varying loads [23]; the verification of the control system through ground and flight test were presented. Yin proposed a neural network sliding mode control method to realize attitude control of a quad tilt rotor aircraft [24]. Moreover, the simulation results were compared with other nonlinear control algorithms to show the feasibility of the proposed method. However, due to the chattering problem, the stability of the SMC is commonly obtained at the cost of sacrificing the nominal control performance. Yang proposed a nonsingular terminal sliding mode controller (NTSMC) combined with neural network (NN) approximation to track the commanded trajectory for robotic airships [25]. The simulation results indicated that NN-NTSMC reduces chattering effectively and ensures faster convergence and better tacking precision against linear hyperplane-based sliding mode control. For a class of nonlinear system, Fu designed a sliding mode controller with unidirectional auxiliary surfaces, and the closed loop stability was proved under the chattering-free condition [26]. By considering the above, to improve robustness without sacrificing control performance, an auxiliary system and disturbance observer can be considered in the SMC scheme design of the tilt-rotor UAVs.

Besides, due to the actual actuator dynamics, the tilt rotor UAVs are constantly affected by the constraints of the inputs. However, there is little research on the flight control of the tilt-rotor UAVs that takes this practical problem into account. To deal with the input constraints, some works on saturated nonlinear control were developed. Li proposed an adaptive robust saturated control strategy for a nonlinear quad rotor system with actuator saturation [27], and an emendatory tracking error was developed to reduce the influence of control inputs on the tracking performance. Zhu designed a nonlinear controller for trajectory tracking of a helicopter with constraints on main thrust and fuselage attitude [28]. Sun adopted a dynamic auxiliary system in the controller of a missile-target interception guidance system for compensating the effects of constrained inputs [29], and the simulation results demonstrate that the robustness of the proposed method is effectively improved. In view of this, a SMC method with auxiliary system can be an effective solution to the control design of the tilt rotor UAVs with input constraints.

Based on the above analysis, this paper aims to design a control scheme consisting of a sliding mode control and auxiliary dynamic (SMC-AD) for a tilt tri-rotor UAV with constrained inputs. The control system adopts cascade control strategy, which is composed of position loop and attitude loop. In the position loop, as is the same for the practical problem of input constraints, a SMC controller with an auxiliary dynamic system is designed. In the attitude loop, the SMC approach is chosen to achieve stable control performance, and a disturbance observer is applied to alleviate the chattering and the influence caused by parameter perturbation and unknown external disturbances. Besides, the control allocation mapping the inputs of the actuators to the outputs of the designed cascade controller, is completed by transforming it into a constrained optimization problem. The main contributions are enumerated as follows.

(i) A nonlinear sliding mode control scheme, composed of a SMC with auxiliary dynamic (SMC-AD) in the position-loop and a SMC with disturbance observer in the attitude loop, is proposed for a tilt tri-rotor UAV. This method is the early application in solving the flight control of the tilt tri-rotor UAV with constrained inputs. Meanwhile, the nonlinearity, parameter perturbations and other unknown external disturbances are also considered in the control scheme. The stability of the overall system is proven mathematically and the effectiveness is verified by simulations and experiment.

(ii) In order to solve the inconsistency between the number of the virtual control quantity and the actual actuators, a control allocation method based on optimization algorithm is developed for the tilt tri-rotor UAV to obtain high control precision.

The tilt tri-rotor UAV has three flight modes, including the hover mode, the fixed-wing mode, and the transition mode. In the stage of vertical take-off and landing, it is necessary to design a good hover mode controller to ensure the stability of the flight process and the accuracy of take-off and landing. In the transition mode, a hybrid controller is commonly used, which is realized by

the weight distribution of the hover mode controller and the fixed wing controller. Thus, the flight control of the hover mode is the premise of realizing the whole process of flight. In this paper, we will focus on the flight control of the tilt tri-rotor UAV in the hover mode. The remaining sections are arranged as follows. Section 2 describes the prototype and mathematical model of the tilt tri-rotor UAV. Section 3 states the main results in detail, including the design of the cascade controller, control allocation, and the stability analysis. Section 4 performs some simulations and experiments to verify the theoretical results. Section 5 draws the final conclusions.

2. Model of the Tilt Tri-Rotor UAV

2.1. Description of the Tilt Tri-Rotor UAV

The proposed tilt tri-rotor UAV is shown in Figure 1. The tilt tri-rotor UAV adopts conventional double tail layout and it has six actuators including three rotors and three tilting steering gears. The rotors are connected with the main structural parts to make the aircraft structurally firm. The three rotors can be tilted from 30° to −90° by the tilting the steering gears for realizing the mode transition between the hover mode and the fixed wing mode. In the hover mode, the rear rotor is set vertically on the tail strut to provide upward tension, which is used to adjust the flight attitudes of the aircraft. The right rotor and rear rotor rotate in counterclockwise while the left in clockwise. Roll motion is achieved by the difference of the thrust between the left and right rotors. The rear rotor can compensate the moment generated by two front rotors to stabilize the pitch, and the yaw moment is produced by the difference between the tilting angles of the two front rotors.

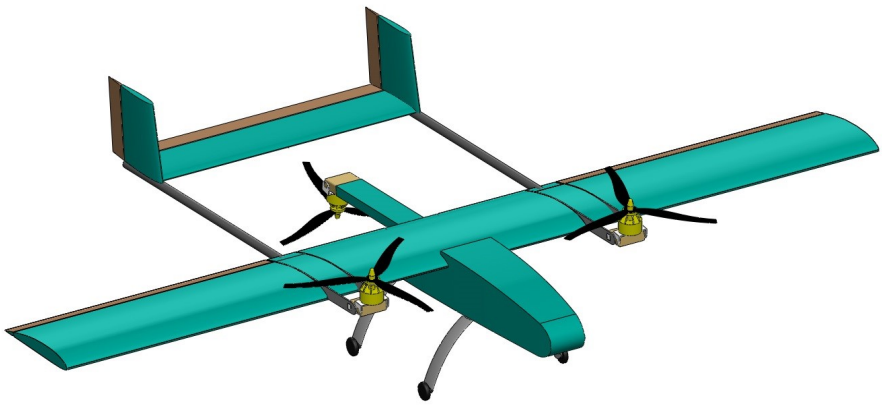

Figure 1. Schematic diagram of the tilt tri-rotor unmanned aerial vehicle (UAV).

2.2. Nonlinear Equations of Motion

In this part, we focus on deriving the 6-DOF nonlinear mathematical model of the tilt tri-rotor UAV. Assuming the UAV as a rigid body, the dynamic model can be derived based on Newton–Euler formulation. The schematic diagram of the tilt tri-rotor UAV coordinate system is shown in Figure 2. $O_eX_eY_eZ_e$ is the world frame, $O_bX_bY_bZ_b$ is the body frame, and $O_rX_rY_rZ_r$ is the rotor frame. It is noted that the right rotor, the left rotor, and the rear rotor are labeled by 1, 2, and 3, respectively. The transformation from the rotor frame to the body frame is done using the matrix R_{ri}^b as follows,

$$R_{ri}^b = \begin{bmatrix} \cos\alpha_i & 0 & \sin\alpha_i \\ 0 & 1 & 0 \\ \sin\alpha_i & 0 & \cos\alpha_i \end{bmatrix} i = 1,2 \quad (1)$$

$$R_{r3}^{b} = \begin{bmatrix} 1 & 0 & 0 \\ 0 & 1 & 0 \\ 0 & 0 & 1 \end{bmatrix} \tag{2}$$

where α_i represents the tilting angle of rotor i, and it is defined as -90° if the UAV is in the hover mode.

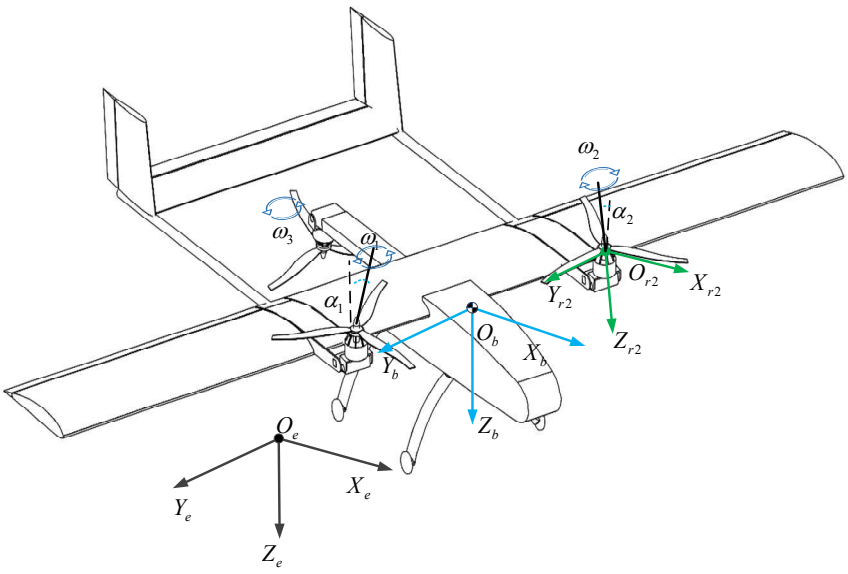

Figure 2. Tilt tri-rotor UAV coordinate system.

In the hover mode, the aerodynamic forces are small enough compared to the thrust and the gravity so that they can be ignored. The resultant force of the tilt tri-rotor UAV F^b includes the rotor thrust F_r^b and the gravity F_g^b.

$$F^b = F_g^b + F_r^b \tag{3}$$

where

$$F_g^b = R_{EBT} \begin{bmatrix} 0 \\ 0 \\ mg \end{bmatrix} \tag{4}$$

$$F_r^b = -R_{r1}^b \begin{bmatrix} 0 \\ 0 \\ k_f \omega_1^2 \end{bmatrix} - R_{r2}^b \begin{bmatrix} 0 \\ 0 \\ k_f \omega_2^2 \end{bmatrix} - R_{r3}^b \begin{bmatrix} 0 \\ 0 \\ k_f \omega_3^2 \end{bmatrix} \tag{5}$$

$$R_{EBT} = \begin{bmatrix} \cos\theta\cos\psi & \cos\theta\sin\psi & -\sin\theta \\ \sin\phi\sin\theta\cos\psi - \cos\phi\sin\psi & \sin\phi\sin\theta\sin\psi + \cos\phi\cos\psi & \sin\phi\cos\theta \\ \cos\phi\sin\theta\cos\psi + \sin\phi\sin\psi & \cos\phi\sin\theta\sin\psi - \sin\phi\cos\psi & \cos\phi\cos\theta \end{bmatrix} \tag{6}$$

where R_{EBT} denotes the transformation matrix from the world frame to the body frame. The mass of the UAV is expressed as m, g is the gravitational acceleration, and ω_i represents the rotational angular velocity of rotor i. The parameter k_f is pull coefficient of the rotor. The total moment τ^b consists of the moment τ_d^b created by the thrust of rotors, the reaction torque of rotors τ_F^b and the moment τ_G^b created by the gyroscopic effect of the propellers, and the body [30]:

$$\tau^b = \tau_F^b + \tau_d^b + \tau_G^b \tag{7}$$

where

$$\tau_F^b = \begin{bmatrix} r_{1x} \\ r_{1y} \\ r_{1z} \end{bmatrix} \times \begin{bmatrix} -k_f\omega_1^2 \sin\alpha_1 \\ 0 \\ -k_f\omega_1^2 \cos\alpha_1 \end{bmatrix} + \begin{bmatrix} r_{2x} \\ r_{2y} \\ r_{2z} \end{bmatrix} \times \begin{bmatrix} -k_f\omega_2^2 \sin\alpha_2 \\ 0 \\ -k_f\omega_2^2 \cos\alpha_2 \end{bmatrix} + \begin{bmatrix} r_{3x} \\ r_{3y} \\ r_{3z} \end{bmatrix} \times \begin{bmatrix} 0 \\ 0 \\ -k_f\omega_3^2 \end{bmatrix} \tag{8}$$

$$\tau_d^b = R_{r1}^b \begin{bmatrix} 0 \\ 0 \\ k_d\omega_1^2 \end{bmatrix} + R_{r2}^b \begin{bmatrix} 0 \\ 0 \\ -k_d\omega_2^2 \end{bmatrix} + R_{r3}^b \begin{bmatrix} 0 \\ 0 \\ k_d\omega_3^2 \end{bmatrix} \tag{9}$$

In Equations (7) and (8), $[r_{ix}, r_{iy}, r_{iz}]^T$ denotes the position of rotor i in the body frame, and k_d is torque coefficient of the rotor. The components of the gyroscopic moment are complicated due to the tilting motion of the rotors, so it is necessary to analyze the gyroscopic moment separately. The changes of the attitude influences the gyroscopic moment of the rear rotor. The gyroscopic moment of the front rotors is not only related to the change of the attitudes but also the tilting motion. Gyroscopic moment of the rotors can be written as

$$\tau_G^b = \tau_{G1}^b + \tau_{G2}^b + \tau_{G3}^b \tag{10}$$

$$\begin{aligned} \tau_{G1}^b = J_1\overrightarrow{\omega_1} \times \overrightarrow{\omega_b} + J_1\overrightarrow{\omega_1} \times \overrightarrow{\omega_{s1}} &= J_1\omega_1 \begin{bmatrix} -\sin\alpha_1 \\ 0 \\ -\cos\alpha_1 \end{bmatrix} \times \begin{bmatrix} p \\ q+\omega_{s1} \\ r \end{bmatrix} \\ &= J_1\omega_1 \begin{bmatrix} (q+\omega_{s1})\cos\alpha_1 \\ -p\cos\alpha_1 + r\sin\alpha_1 \\ -(q+\omega_{s1})\sin\alpha_1 \end{bmatrix} \end{aligned} \tag{11}$$

$$\begin{aligned} \tau_{G2}^b = J_2\overrightarrow{\omega_2} \times \overrightarrow{\omega_b} + J_2\overrightarrow{\omega_2} \times \overrightarrow{\omega_{s2}} &= J_2\omega_2 \begin{bmatrix} \sin\alpha_2 \\ 0 \\ \cos\alpha_2 \end{bmatrix} \times \begin{bmatrix} p \\ q+\omega_{s2} \\ r \end{bmatrix} \\ &= J_2\omega_2 \begin{bmatrix} -(q+\omega_{s2})\cos\alpha_2 \\ p\cos\alpha_2 - r\sin\alpha_2 \\ (q+\omega_{s2})\sin\alpha_2 \end{bmatrix} \end{aligned} \tag{12}$$

$$\tau_{G3}^b = J_3\overrightarrow{\omega_3} \times \overrightarrow{\omega_b} = J_3\omega_3 \begin{bmatrix} q \\ -p \\ 0 \end{bmatrix} \tag{13}$$

where J_i is the moment of inertia of the rotor i, $\overrightarrow{\omega_b} = [p, q, r]^T$ represents the rotational angular velocity in the body frame, and $\overrightarrow{\omega_{si}}$ is the tilting angular velocity of rotor i.

According to the Newton–Euler formulation [31], the translational and rotational motion equations of the tilt tri-rotor UAV are derived as

$$\begin{cases} \dot{\chi} = V \\ m\dot{V} = mge_3 - R_{BET}Te_3 + d_F \\ \dot{\Theta} = R_{BER} \cdot \omega_b \\ I_b\dot{\omega}_b = \Gamma - \omega_b \times (I_b \cdot \omega_b) + d_\Gamma \end{cases} \tag{14}$$

where $\chi = [X, Y, Z]^T$ and $V = [u, v, w]^T$ are the position and linear velocity of the vehicle center in the world frame, respectively. Note that $e_3 = [0, 0, 1]^T$ is a constant vector, T is the virtual control force, $\Gamma = [R, P, Y]^T$ is the virtual control torque, d_F and d_Γ represent the external disturbances, $\Theta = [\phi, \theta, \psi]^T$ is the Euler angle, I_b is the inertial matrix with respect to the body coordinate system, R_{BET} is the

velocity transformation matrix from the body frame to the world frame, and the rotation matrix from the body frame to the world frame is R_{BER}.

$$R_{BET} = R_{EBT}^{T}, R_{BER} = \begin{bmatrix} 1 & \sin\phi\tan\theta & \cos\phi\tan\theta \\ 0 & \cos\phi & -\sin\phi \\ 0 & \frac{\sin\phi}{\cos\theta} & \frac{\cos\phi}{\cos\theta} \end{bmatrix} \tag{15}$$

Based on the above analysis, the mathematical model of the tilt tri-rotor UAV is obtained.

3. Flight Controller Design

The tilt tri-rotor UAV is a novel aircraft with unique structure, resulting in a challenging control problem. The block diagram of the proposed flight control system is shown in Figure 3. The flight control system consists of two parts: the cascade controller and the control allocator. The cascade controller generates the virtual control quantities of the position and attitude control. The outer-loop is used for position control, and the inner-loop handles the attitude control of the tilt tri-rotor UAV. The control allocator, which maps the virtual control command to individual actuators, is used to deal with the problem of mismatch between the numbers of the virtual control quantities and the actual actuators.

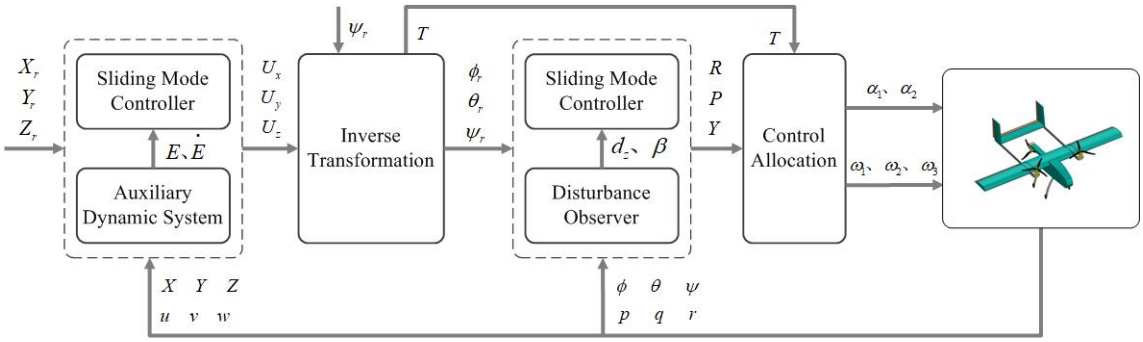

Figure 3. Block diagram of the flight control system.

In the position control loop of the cascade controller, to ensure the trajectory tracking error converges to zero asymptotically, we choose the auxiliary dynamic system based SMC approach to design a saturated control input $U_p = [U_x, U_y, U_z]^T$, which can limit the magnitude of the thrust and the reference signal of pitch and roll motion of the attitude loop. Then, we utilize the SMC approach with a disturbance observer for the attitude loop to address the model uncertainties and disturbances. Besides, an optimization algorithm based control allocation is developed to obtain high control precision.

3.1. Position Controller Design

The position control is realized by the adjustment of the UAV's attitudes. The desired roll angle ϕ_r and pitch angle θ_r given by the position controller are the reference inputs for the attitude controller. The input of the position controller is the position reference signal $\chi_r = [X_r, Y_r, Z_r]^T$, while the output consists of the virtual thrust U_p. The desired attitude ϕ_r, θ_r and thrust T can be obtained using the inverse transformation. The design of the position controller is divided into two steps, the first step is to design control law based on adaptive SMC-AD approach, and the second step is to solve the desired angles and thrust from the control law that is designed in the first step.

Similar to a conventional vehicle, the tilt tri-rotor UAV has four virtual control quantities R, P, Y and T, where R is directly linked to roll control, P is used for pitch control, Y is related to yaw control, and the altitude is controlled by T. The objective of this section is to develop control outputs T and $\Gamma = [R, P, Y]^T$ for the tilt tri-rotor UAV. Define the position error $\chi_e = \chi_r - \chi$, the virtual position error

$\chi_{ee} = \chi_e - E$, the velocity error $V_e = V_r - V$, and the virtual velocity error $V_{ee} = V_e - \dot{E}$, where E is an auxiliary variable. The virtual thrust is represented by $U_p = -R_{BET}Te_3$. Based on (14), the virtual error dynamics of the position subsystem can be given by

$$\begin{cases} \dot{\chi}_{ee} = V_{ee} \\ m\dot{V}_{ee} = m\ddot{\chi}_r - (U_p + mge_3 + d_F) - m\ddot{E} \end{cases} \tag{16}$$

Theorem 1. *The position error subsystem in (16) can be asymptotically stabilized if the virtual thrust and the second-order auxiliary dynamic system are defined as follows,*

$$U_p = m(\ddot{\chi}_r - ge_3 + k_\alpha \tanh(kE + l\dot{E}) + k_\beta \tanh(l\dot{E})) \tag{17}$$

$$\ddot{E} = -k_\alpha \tanh(kE + l\dot{E}) - k_\beta \tanh(l\dot{E}) + k_p V_{ee} + \frac{c_p}{m} s_p + \frac{\varepsilon_p}{m} \operatorname{sgn}(s_p) \tag{18}$$

where $s_p = k_p\chi_{ee} + V_{ee}$ is a classical sliding manifold, and k_p, c_p, ε_p, k_α, k_β, k, and l are positive constants.

Proof. At first, consider the following Lyapunov candidate for position subsystem

$$V_p = \frac{m}{2} s_p^T s_p \tag{19}$$

The derivative of the Lyapunov function is then obtained by

$$\begin{aligned} \dot{V}_p &= m s_p^T \dot{s}_p \\ &= s_p^T (m k_p V_{ee} + m\ddot{\chi}_r - (U_p + mge_3 + d_F) - m\ddot{E}) \end{aligned} \tag{20}$$

Substituting (17) and (18) into (20) yields

$$\dot{V}_p = -s_p^T c_p s_p - s_p^T \varepsilon_p \operatorname{sgn}(s_p) - s_p^T d_F \tag{21}$$

If the value of ε_p is large enough $\varepsilon_p > \|d_F\|$, it can be concluded that

$$\dot{V}_p = -s_p^T c_p s_p - s_p^T \varepsilon_p \operatorname{sgn}(s_p) - s_p^T d_F \leq 0 \tag{22}$$

As $V_p \geq 0$ and $\dot{V}_p \leq 0$, $\dot{V}_p = 0$ only if $s_p = 0$. Therefore, we can conclude that V_p is monotonically decreasing and can converge to zero in finite time. According to (19), we have $s_p = 0$.

$$k_p\chi_{ee} + V_{ee} = 0 \tag{23}$$

Substituting (16) into (23) yields

$$\dot{\chi}_{ee} = -k_p\chi_{ee} \tag{24}$$

From (24), we have

$$\chi_{ee} = e^{-k_p t}\chi_{ee}(0) \tag{25}$$

where $\chi_{ee}(0)$ denotes the initial error. Because k_p is a positive parameter, the tracking errors χ_{ee} and V_{ee} of the nominal position error subsystem (16) are asymptotically stable. □

Theorem 2. *The auxiliary dynamic system (18) is asymptotically stable.*

Proof. The auxiliary system can be rewritten as

$$\ddot{E} = -k_\alpha \tanh(kE + l\dot{E}) - k_\beta \tanh(l\dot{E}) + \Delta \tag{26}$$

where $\Delta = k_p V_{ee} + \frac{c_p}{m} s_p + \frac{\varepsilon_p}{m} \operatorname{sgn}(s_p)$ can be regarded as a disturbance term. Moreover, the nominal auxiliary system without the disturbance term is given as

$$\begin{cases} \dot{E}_1 = E_2 \\ \dot{E}_2 = -k_\alpha \tanh(kE_1 + lE_2) - k_\beta \tanh(lE_2) \end{cases} \tag{27}$$

Based on the proof given above, the disturbance term Δ converges to zero asymptotically. We focus on proving the convergence of the nominal auxiliary system. Considering the Lyapunov candidate function

$$L = k_\alpha \ln(\cosh(kE_1 + lE_2)) + k_\beta \ln(\cosh(lE_2)) + \frac{kE_2^2}{2} \tag{28}$$

According to the (27), we have

$$\begin{aligned} \dot{L} &= k_\alpha \tanh(kE_1 + lE_2)^T (k\dot{E}_1 + l\dot{E}_2) + k_\beta l \tanh(lE_2)^T \dot{E}_2 + kE_2^T \dot{E}_2 \\ &= -l[k_\alpha \tanh(kE_1 + lE_2) + k_\beta \tanh(lE_2)]^T [k_\alpha \tanh(kE_1 + lE_2) + k_\beta \tanh(lE_2)] - kk_\beta E_2^T \tanh(lE_2) \\ &\leq 0 \end{aligned} \tag{29}$$

Only if $E_1 = 0$ and $E_2 = 0$, we have $\dot{L} = 0$. As a result, the asymptotical stability of the nominal auxiliary system is proved. □

As the states χ_{ee}, V_{ee}, $\dot{E}$, and $\ddot{E}$ are asymptotically stable, we can conclude that the proposed position controller can guarantee the asymptotic stability of the tracking errors χ_e and V_e.

The exponential approach law is introduced to improve control performance. However, due to the existence of non-ideality in the practical implementation of $\operatorname{sgn}(s_p)$, the chattering problem may not be ignored. To overcome the problem for the position subsystem, $\operatorname{sgn}(s_p)$ can be substituted by the hyperbolic tangent function

$$\tanh(\frac{s_p}{\rho_p}) = \frac{e^{\frac{s_p}{\rho_p}} - e^{-\frac{s_p}{\rho_p}}}{e^{\frac{s_p}{\rho_p}} + e^{-\frac{s_p}{\rho_p}}} \tag{30}$$

where the parameter ρ_p is selected by considering the trade-off between the hardware capability and the control accuracy and robustness.

The virtual thrust $U_p = [U_x, U_y, U_z]^T$ is derived above, then the thrust T, the desired roll angle ϕ_r, and the pitch angle θ_r can be extracted. It should be mentioned that the aircraft can provide thrust T_{actual} along the z-axis of the body coordinate system during the hover mode.

$$\begin{cases} U_x = -T(\cos\phi \sin\theta \cos\psi + \sin\phi \sin\psi) \\ U_y = -T(\cos\phi \sin\theta \sin\psi - \sin\phi \cos\psi) \\ U_z = -T \cos\phi \cos\theta \end{cases} \tag{31}$$

The desired yaw angle ψ_r is given by the user input device or trajectory planner in advance, then we have

$$\begin{cases} \theta_r = \arctan(\dfrac{U_x \cos\psi_r + U_y \sin\psi_r}{U_z}) \\ \phi_r = \arctan(\dfrac{\cos\theta_r (U_x \sin\psi_r - U_y \cos\psi_r)}{U_z}) \\ T = -\dfrac{U_z}{\cos\theta_r \cos\phi_r} \end{cases} \tag{32}$$

Remark 1. *By introducing the auxiliary dynamic system, the virtual thrust U_p is bounded. Furthermore, the thrust T and desired angles ϕ_r, θ_r are constrained to a safe range.*

According to (17), the amplitude of the virtual thrust U_p mainly depends on the desired acceleration $\ddot{\chi}_r$. In general, $\ddot{\chi}_r$ cannot be too large; therefore, the virtual thrust U_p is bounded and satisfies

$$\|U_p\| \leq m(\|\ddot{\chi}_r\| + \|ge_3\| + \sqrt{3}(k_\alpha + k_\beta)) \tag{33}$$

From (31), it is clear that $T = \|U_p\|$. Given that the desired acceleration $\ddot{\chi}_r$ and control parameters k_α, k_β, it is obvious that the thrust T satisfies

$$T \leq m(\|\ddot{\chi}_r\| + g + \sqrt{3}(k_\alpha + k_\beta)) \tag{34}$$

For the plane motion, the virtual thrust U_x and U_y are provided by (17), we can also conclude that

$$\begin{cases} U_x \leq m(|\ddot{\chi}_{rx}| + k_\alpha + k_\beta) \\ U_y \leq m(|\ddot{\chi}_{ry}| + k_\alpha + k_\beta) \end{cases} \tag{35}$$

The virtual thrust U_z is used for altitude control in the world frame, so the value of U_z is approximately equal to the gravity. It is the main component of U_p. Taking (32) into consideration, we can conclude that the desired roll and pitch angles are bounded.

3.2. Attitude Controller Design

The purpose of the attitude controller is to the derive the virtual torque $\Gamma = [R, P, Y]^T$ from the desired attitude, which is given as $\Theta_r = [\phi_r, \theta_r, \psi_r]^T$. To achieve stable and robust control, a SMC approach based on disturbance observer that we have proposed before [32] is used to calculate the control law for the attitude control subsystem. In this method, the SMC part is to produce a robust control law and the disturbance observer is adopted to deal with the modeling errors and the external disturbances.

Based on (14), the attitude control subsystem can be rewritten as follows [33],

$$J(\Theta)\ddot{\Theta} = -C(\Theta, \dot{\Theta})\dot{\Theta} + \Gamma + d_\Gamma + \triangle_p \tag{36}$$

$$J(\Theta) = \begin{bmatrix} I_{xx} & 0 & -I_{xx}s\theta \\ 0 & I_{yy}c^2\phi + I_{zz}s^2\phi & (I_{yy} - I_{zz})c\phi s\phi c\theta \\ -I_{xx}s\theta & (I_{yy} - I_{zz})c\phi s\phi c\theta & I_{xx}s^2\theta + I_{yy}s^2\phi c^2\theta + I_{zz}c^2\phi c^2\theta \end{bmatrix} \tag{37}$$

where $\Theta = [\phi, \theta, \psi]^T$ is the actual attitude; $J(\Theta)$ denotes the inertia matrix; $C(\Theta, \dot{\Theta})$ denotes the Coriolis matrix; and d_Γ and $\triangle_p$ represent the external disturbances and the modeling errors, respectively. $c\cdot$ and $s\cdot$ are symbolize cosine and sine function respectively. Generally, the pitch angle satisfies $\theta \in (-\frac{\pi}{2}, \frac{\pi}{2})$, so $J(\Theta)$ is an invertible and positive definite symmetric matrix.

Define the error vector as $x_1 = \Theta_r - \Theta$, $x_2 = \dot{\Theta}_r - \dot{\Theta}$. Then, we can obtain the attitude error system as

$$\begin{cases} \dot{x}_1 = x_2 \\ \dot{x}_2 = J(\Theta)^{-1}[J(\Theta)\ddot{\Theta}_r - (\Gamma + D - C(\Theta, \dot{\Theta})\dot{\Theta})] \end{cases} \tag{38}$$

where $D = d_\Gamma + \triangle_p$ denotes the total effects of the external disturbances and the modeling errors.

Inspired by the work in [34], we denote $\hat{D} = d_e + \beta(x_1, x_2)$ to be the estimated value of D. $d_e \in R^3$ is a dynamic part and $\beta(x_1, x_2)$ is an auxiliary function. Then, the estimation error of D is obtained as

$$\begin{aligned} e &= \hat{D} - D \\ &= d_e + \beta(x_1, x_2) - D \end{aligned} \tag{39}$$

To achieve accurate estimation of D, the nonlinear disturbance observer is designed as follows,

$$\begin{cases} \dot{d}_e = -\dfrac{\partial \beta}{x_1} x_2 - \dfrac{\partial \beta}{x_2} J(\Theta)^{-1}[J(\Theta)\ddot{\Theta}_r - (\Gamma + \hat{D} - C(\Theta, \dot{\Theta})\dot{\Theta})] \\ \beta(x_1, x_2) = -k_2 x_2 \end{cases} \tag{40}$$

where k_2 is a positive constant that related to the convergence speed of the disturbance estimation.

Assume that the disturbance D is a slow time-varying variable compared to the state of the system, so that the derivative of D can be omitted. Then, we can get

$$\begin{aligned} \dot{e} &= \dot{d}_e + \dot{\beta}(x_1, x_2) \\ &= -k_2 J(\Theta)^{-1} e \end{aligned} \tag{41}$$

As $J(\Theta)^{-1}$ is a positive definite symmetric matrix and k_2 is a positive constant, $-k_2 J(\Theta)^{-1}$ is Hurwitz. If k_2 is appropriately chosen, certain disturbance estimation accuracy can be guaranteed. If the actual disturbance is a constant, e converges to 0. If it is a variable, the estimation error exists and satisfies

$$|e| \leq D_e^* = \sup_{t>0} |d_z + \beta(x_1, x_2) - D| \tag{42}$$

Based on the designed disturbance observer above, the following part is to develop the sliding mode controller based on the disturbance observer, such that the chattering is alleviated and the robustness can be improved without sacrificing nominal control performance.

Theorem 3. *To achieve stable control for the attitude subsystem* (38)*, the control law based on SMC approach can be designed as follows [32],*

$$\Gamma = C(\Theta, \dot{\Theta})\dot{\Theta} + J(\Theta)\ddot{\Theta}_r + J(\Theta)k_a(\dot{\Theta}_r - \dot{\Theta}) + c_a s_a + \varepsilon_a \operatorname{sgn}(s_a) - \hat{D} \tag{43}$$

where k_a and c_a are positive constants, $\varepsilon_a > D_e^*$, and the sliding manifold is $s_a = k_a x_1 + x_2$.

Proof. The derivative of the sliding mode surface s_a can be written as

$$\begin{aligned} \dot{s}_a &= k_a \dot{x}_1 + \dot{x}_2 \\ &= k_a x_2 + J(\Theta)^{-1}[J(\Theta)\ddot{\Theta}_r - (\Gamma + D - C(\Theta, \dot{\Theta})\dot{\Theta})] \end{aligned} \tag{44}$$

Substituting the control law (43) into (44), it yields

$$J(\Theta)\dot{s}_a = -c_a s_a - \varepsilon_a \operatorname{sgn}(s_a) + e \tag{45}$$

Consider a candidate Lyapunov function as

$$V_a = \frac{1}{2} s_a^T s_a \tag{46}$$

the derivative of the Lyapunov function along (45) satisfies

$$\dot{V}_a = s_a^T \dot{s}_a \tag{47}$$

$$= s_a^T J(\Theta)^{-1}[-c_a s_a - \varepsilon_a \operatorname{sgn}(s_a) + e] \tag{48}$$

As $\varepsilon_a > D_e^*$, we have

$$\dot{V}_a < -s_a^T J(\Theta)^{-1} c_a s_a \leq 0 \tag{49}$$

It indicates that the sliding mode surface s_a can converge to the equilibrium point asymptotically under the proposed control law (43). As the reachability condition of sliding mode surface is satisfied, the attitude control subsystem (38) is asymptotically stable when $k_a x_1 + x_2 = 0$. □

Remark 2. *Due to the application of the disturbance observer, the estimation error e is much smaller than the upper bound of D_e^*. As for the switch gain ε_a, it can be set much smaller than the conventional SMC approach. As a result, the chattering is alleviated and robustness can be improved without sacrificing the nominal control performance.*

3.3. Control Allocation

In this section, the design of the control allocation algorithm, which provides the mapping from the virtual control quantities to the manipulated inputs of the UAV, is presented. In the hover mode, the tilt tri-rotor UAV has five actuators that consist of three rotors and two servos, and the attitude and position are controlled by these five actuators. In order to achieve stable flight control, a control allocator-based optimization algorithm is proposed.

From Figure 3, there are five outputs $[\omega_1, \omega_2, \omega_3, \alpha_1, \alpha_2]$ to be solved by four inputs $[R, P, Y, T]$ in the control allocator, and the number of unknowns is greater than the number of equations, so it can be treated as an optimization problem. To solve this problem, a cost function which is related to the consumption of power is proposed as follows,

$$J = \omega_1^4 + \omega_2^4 + \omega_3^4 \tag{50}$$

Moreover, it can be rewritten as

$$J = U_1^2 + U_2^2 + U_3^2 + U_4^2 + U_5^2 \tag{51}$$

where

$$\begin{cases} U_1 = \omega_1^2 \cos\alpha_1 \\ U_2 = \omega_1^2 \sin\alpha_1 \\ U_3 = \omega_2^2 \cos\alpha_2 \\ U_4 = \omega_2^2 \sin\alpha_2 \\ U_5 = \omega_3^2 \end{cases} \tag{52}$$

The solving of these nonlinear coupled equations is transformed into a constrained optimization problem.

$$\begin{aligned} &min \;\; J = U_1^2 + U_2^2 + U_3^2 + U_4^2 + U_5^2 \\ &s.t \begin{cases} -k_f U_1 r_{1y} + k_d U_2 - k_f U_3 r_{2y} - k_d U_4 - R = 0 \\ k_f U_1 r_{1x} + k_f U_3 r_{2x} + k_f U_5 r_{3x} - P = 0 \\ k_f (U_2 r_{1y} + U_4 r_{2y}) + k_d (U_1 - U_3 + U_5) - Y = 0 \\ k_f U_1 + k_f U_3 + k_f U_5 - T = 0 \end{cases} \end{aligned} \tag{53}$$

Note that J is a continuously differentiable function. The second-order partial derivative matrix of J is given as

$$\nabla^2 J = 2I \tag{54}$$

$\nabla^2 J$ is a positive definite matrix, so J is a convex function, and the optimization problem can be solved by using the Lagrangian multiplier method [35]. The Lagrange function is defined as

$$\begin{aligned} L =& U_1^2 + U_2^2 + U_3^2 + U_4^2 + U_5^2 \\ &+ \lambda_1(-k_f U_1 r_{1y} + k_d U_2 - k_f U_3 r_{2y} - k_d U_4 - R) \\ &+ \lambda_2(k_f U_1 r_{1x} + k_f U_3 r_{2x} + k_f U_5 r_{3x} - P) \\ &+ \lambda_3(k_f(U_2 r_{1y} + U_4 r_{2y}) + k_d(U_1 - U_3 + U_5) - Y) \\ &+ \lambda_4(k_f U_1 + k_f U_3 + k_f U_5 - T) \end{aligned} \tag{55}$$

$$\nabla L(U) = 2U + \Sigma\Lambda = 0 \tag{56}$$

where $U = [U_1, U_2, U_3, U_4, U_5]^T$ and $\Lambda = [\lambda_1, \lambda_2, \lambda_3, \lambda_4]^T$.

$$\Sigma = \begin{bmatrix} -k_f r_{1y} & k_f r_{1x} & k_d & k_f \\ k_d & 0 & k_f r_{1y} & 0 \\ -k_f r_{2y} & k_f r_{2x} & -k_d & k_f \\ -k_d & 0 & k_f r_{2y} & 0 \\ 0 & k_f r_{3x} & k_d & k_f \end{bmatrix} \tag{57}$$

The equality constraints in (53) can be rewritten as

$$\zeta U = C \tag{58}$$

where $C = [R, P, Y, T]^T$.

$$\zeta = \begin{bmatrix} -k_f r_{1y} & k_d & -k_f r_{2y} & -k_d & 0 \\ k_f r_{1x} & 0 & k_f r_{2x} & 0 & k_f r_{3x} \\ k_d & k_f r_{1y} & -k_d & k_f r_{2y} & k_d \\ k_f & 0 & k_f & 0 & k_f \end{bmatrix} \tag{59}$$

Because ζ is not a square matrix, from (56) and (58), we can obtain

$$\Lambda = -2(\zeta\Sigma)^{-1}C \tag{60}$$

$$U = \Sigma(\zeta\Sigma)^{-1}C \tag{61}$$

Therefore, the values of the actual outputs are given as

$$\begin{cases} \omega_1^2 = \sqrt{U_1^2 + U_2^2} \\ \omega_2^2 = \sqrt{U_3^2 + U_4^2} \\ \omega_3^2 = U_5 \\ \alpha_1 = \arctan(\dfrac{U_2}{U_1}) \\ \alpha_2 = \arctan(\dfrac{U_4}{U_3}) \end{cases} \tag{62}$$

The proposed control allocation algorithm can improve the control accuracy with less power consumption.

4. Simulations and Experimental Test

To verify the performance of the proposed control scheme, numerical simulations are carried out on a tilt tri-rotor UAV with the aircraft structure shown in Figure 1. All the simulations are completed by using MATLAB/SIMULINK software. In the simulations, the performance of the proposed control method is examined in the hover mode for its ability to reject low-frequency disturbances, and the robustness against system parameter variations is also tested. Besides, in order to validate the performance improvement obtained with the proposed control scheme, the proposed SMC-AD control approach is compared with the two other control methods.

The model parameters using in the simulations are obtained by experiments. The oscillation method is used to measure the moments of inertia and the center of gravity [36]. The relationships between the force, moment, and rotation speed of the rotors are also tested by an intelligent ergometer. Based on the experimental results, k_f and k_d is obtained by the least square method [37]. The physical parameters of the tilt tri-rotor UAV are shown in Table 1.

Table 1. Physical parameters.

Symbol	Description	Magnitude
m	mass	5.6 kg
r_{1x}	Right rotor distance along x axis	0.22 m
r_{1y}	Right rotor distance along y axis	0.2635 m
r_{1z}	Right rotor distance along z axis	0 m
r_{3x}	rear rotor distance along x axis	-0.42 m
r_{3y}	rear rotor distance along y axis	0 m
r_{3z}	rear rotor distance along z axis	0 m
I_{xx}	Moment of inertia around x axis	0.3556 kg $\cdot$ m^2
I_{yy}	Moment of inertia around y axis	0.3553 kg $\cdot$ m^2
I_{zz}	Moment of inertia around z axis	0.6084 kg $\cdot$ m^2
k_f	pull coefficient of the rotor	4.531×10^{-5}
k_d	Moment coefficient of the rotor	9.409×10^{-7}

4.1. Performance against Disturbances and Parameters Perturbation

In this part, the proposed control system is assessed regarding robustness and capabilities. On the one hand, the controller is examined for its ability to reject low-frequency disturbances. On the other hand, the robustness against model parameter variations is also tested.

The simulations against the external disturbances are divided into two aspects: the position control and the attitude control. In the simulations of the position control, the process is designed as follows. At 0 s, the UAV takes off and hovers at a given point. At 5 s and 10 s, the position step signal with the amplitude of 1m is introduced in the Y and X direction. Then, a low-frequency sinusoidal disturbance is applied to the three channels of the position subsystem at 8–10 s, 12–14 s, and 16–18 s, respectively. The magnitude of the low-frequency sinusoidal disturbance is 5 N, and can be given as

$$d_x(t) = \begin{cases} 5sin(\pi(t-16)), & 16 \le t \le 18 \\ 0, & t < 16, t > 18 \end{cases} \tag{63}$$

$$d_y(t) = \begin{cases} 5sin(\pi(t-12)), & 12 \le t \le 14 \\ 0, & t < 12, t > 14 \end{cases} \tag{64}$$

$$d_z(t) = \begin{cases} 5sin(\pi(t-8)), & 8 \le t \le 10 \\ 0, & t < 8, t > 10 \end{cases} \tag{65}$$

Figure 4 shows the tracking curves of the position control subsystem. Moreover, the disturbances are scaled to one-tenth to be shown in the figure, so that the influence of the external disturbance can be demonstrated clearly. After the step signal is applied to the UAV in the X and Y directions, the position controller can make the errors of two channels converge to zero in ~3 s. When the sinusoidal disturbances are introduced into the three directions, the position errors begin to increase. It is noteworthy that the curve of position X almost coincides with Y, and the position error of the two curves caused by the disturbances is less than 0.1 m. However, the curve of Z almost has no change. The simulation results are consistent with the proposed control strategy. The altitude is controlled by the thrust directly. Meanwhile, the position control in X-axis and Y-axis are achieved by the adjustment of the attitudes.

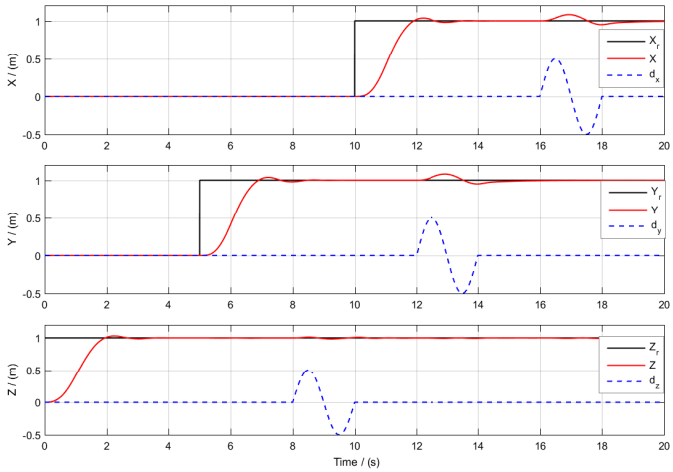

Figure 4. Position variations under the disturbances (X, Y, Z).

As for the simulations of the attitude tracking and external disturbances suppression of the attitude controller, we make the UAV hover at a set point and set a sinusoidal reference signal in the three directions at 0–4 s, 6–10 s, and 12–16 s, respectively. Besides, a sinusoidal disturbance torque with amplitude of 3 N·m is added to the three directions at 8–10 s, 12–14 s, and 16–18 s, respectively. The sinusoidal disturbance torque is given as

$$d_\phi(t) = \begin{cases} 3sin(\pi(t-8)), & 8 \le t \le 10 \\ 0, & t < 8, t > 10 \end{cases} \tag{66}$$

$$d_\theta(t) = \begin{cases} 3sin(\pi(t-12)), & 12 \le t \le 14 \\ 0, & t < 12, t > 14 \end{cases} \tag{67}$$

$$d_\psi(t) = \begin{cases} 3sin(\pi(t-16)), & 16 \le t \le 18 \\ 0, & t < 16, t > 18 \end{cases} \tag{68}$$

Figure 5 shows the tracking curves of the attitude control subsystem, and the disturbances are also scaled to one-tenth shown in the figure. From Figure 5, it can be seen that the attitudes can track the reference signal well. When the sinusoidal disturbance torques are added, the controller can quickly suppress the influence of external disturbances, and the attitude almost does not change. Besides, due to the use of the disturbance observer, there is no chattering caused by the sliding mode controller.

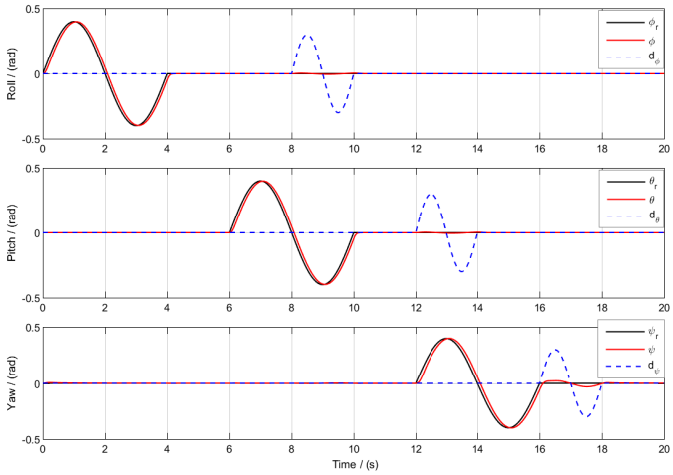

Figure 5. Attitude variations under the disturbances (ϕ, θ, ψ).

In order to verify the robustness of the proposed control system, several significant model parameters are changed as shown in Table 2. The simulation process is reproduced again. Figure 6 gives the position curves under the condition of step signal and external sinusoidal force disturbances. Obviously, the proposed position controller can also ensure the tracking and anti-interference performance of the system when parameters change. Moreover, the tracking curves of the attitude control subsystem under parameter variations are shown in Figure 7. Similarly, the control system ensures the tracking ability and anti-interference ability of the attitude control loop.The results show that the proposed control scheme has good robustness.

Table 2. Variation of model parameters.

Symbol	Variation	Symbol	Variation
m	120%	I_{xx}	120%
k_f	80%	I_{yy}	120%
k_d	80%	I_{zz}	120%

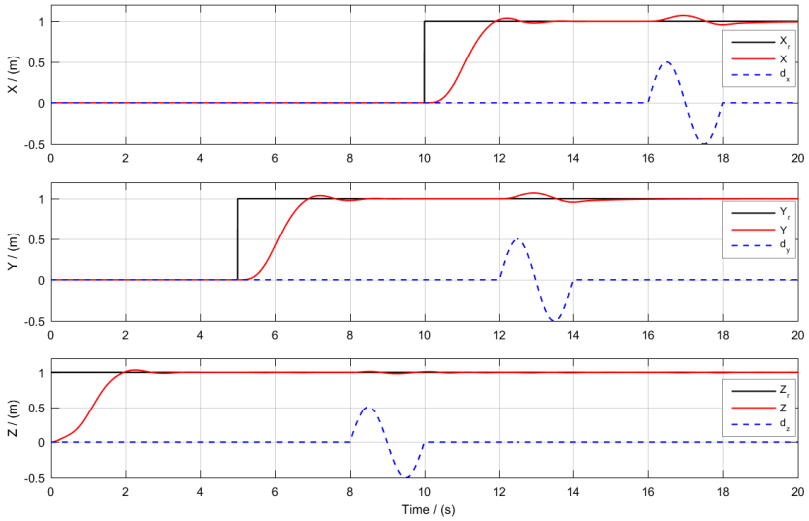

Figure 6. Position variations under the disturbances when parameters change (X, Y, Z).

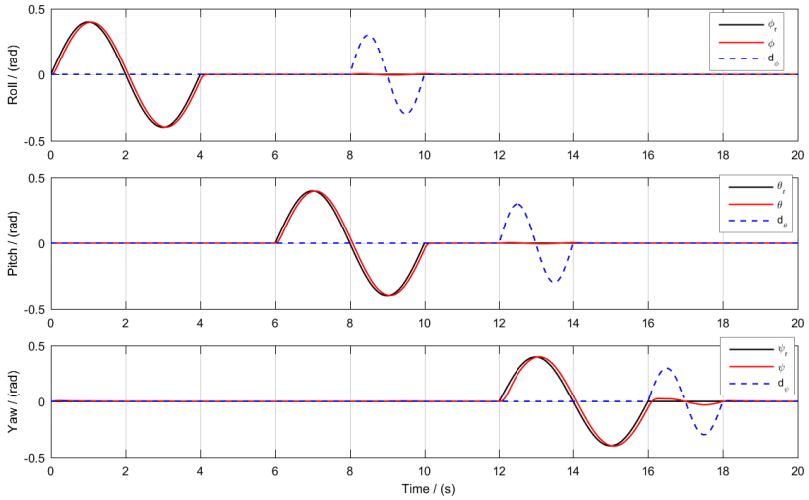

Figure 7. Attitude variations under the disturbances when parameters change (ϕ, θ, ψ).

4.2. Comparisons with Other Methods

In order to show the performance improvement of the proposed control scheme, simulations are conducted by comparing the proposed control scheme with PID control [17] and SMC with radical basic function neural network (SMC-RBFNN) [25]. Among the two control schemes, PID control is the most widely used method in practice, while SMC-RBFNN is also an advanced nonlinear control approach which can alleviate the chattering and improve robustness without sacrificing control performance. The parameters of the three control schemes are given in the Appendix A. The process of the simulations is described as follows.

The whole simulation is completed within 90 s. At first, the UAV spirals up to 80 m in the first 40 s. In the next 10 s, the UAV flights forward the X direction, and a lateral sinusoidal disturbance force with amplitude of 4N is introduced in 45–49 s. Then, the UAV turns right at 50 s and flights forward the Y direction. In 55–59 s, the sinusoidal disturbance of the rolling moment with magnitude of 1.5 N·m is introduced. At 60 s, the UAV turns right and flights forward the opposite direction of the x-axis. In 65–69 s, the sinusoidal disturbance of the pitching moment with magnitude 1.5 N·m is introduced. Finally, the UAV reduces the altitude and lands in the last 20 s. The desired and actual trajectories of the tilt tri-rotor UAV are shown in Figure 8.

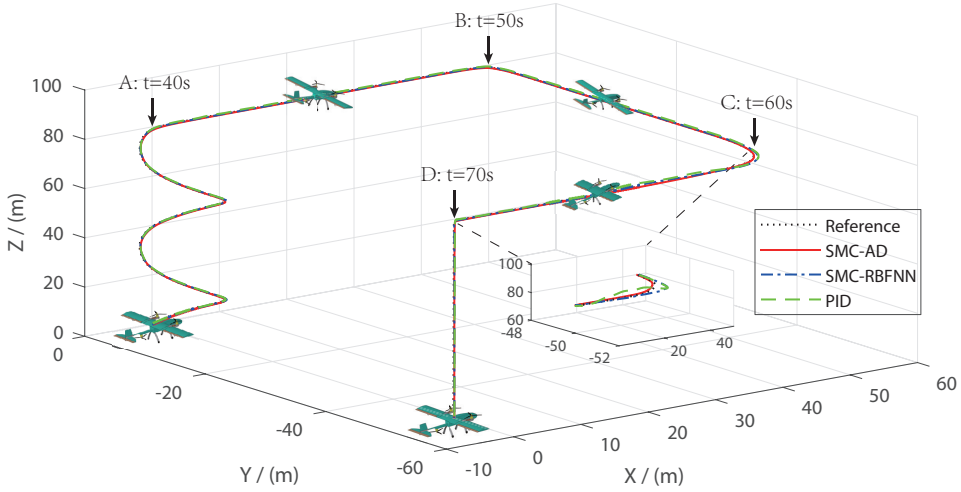

Figure 8. Path following .

The curves of the position, attitude, and the thrust T are depicted in Figures 9–11. In Figure 9, compared with the other methods, the position errors of the proposed SMC-AD control method in this paper always keep a smaller value in the simulation process when the external force or moment disturbances are added. Besides, in the stage of taking off and landing, the proposed control scheme shows better tracking performance. In the aspect of attitude control, Figure 10 show that roll, pitch, and yaw motion can quickly suppress the influence of torque disturbance and track the desired attitude signal by using the proposed method. In the whole simulation process, the PID control show greater attitude vibrations, and the curves of the proposed method are close to that of the SMC-RBFNN control scheme. Figure 11 shows the virtual thrust which is computed by the flight controller. It can be seen that the proposed SMC-AD method successfully restricts the virtual control thrust and the thrust is smaller and smoother than the other two methods. This kind of restriction is very useful in practical applications. Once actuator saturation occurs, the UAV without thrust constraint may be unexpectedly unstable.

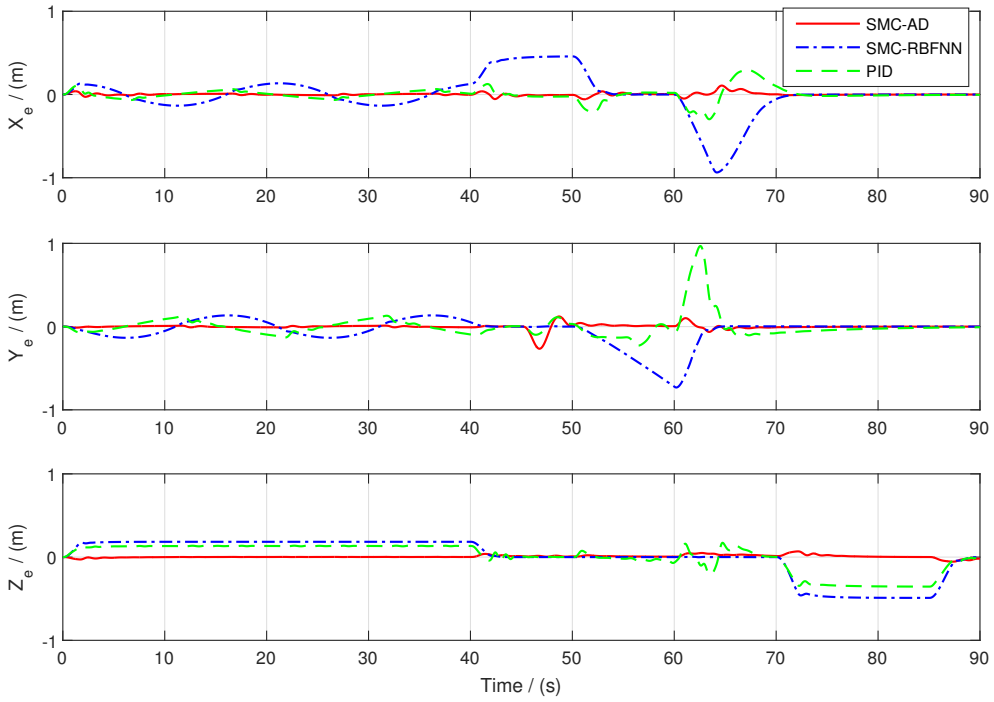

Figure 9. Position error (X_e, Y_e, Z_e).

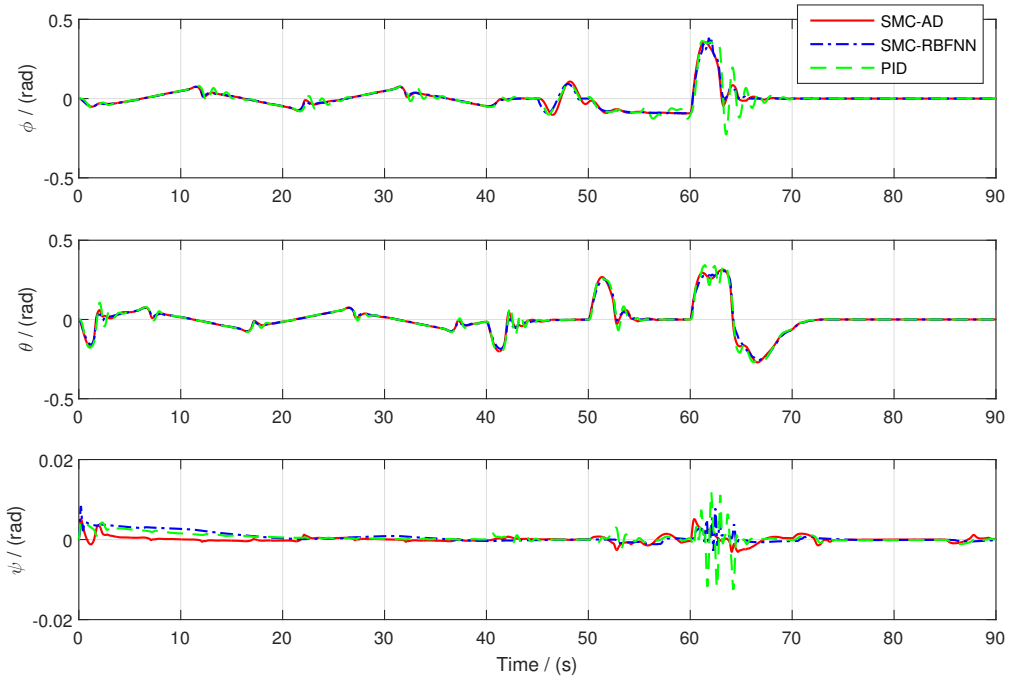

Figure 10. Attitude variations (ϕ, θ, ψ).

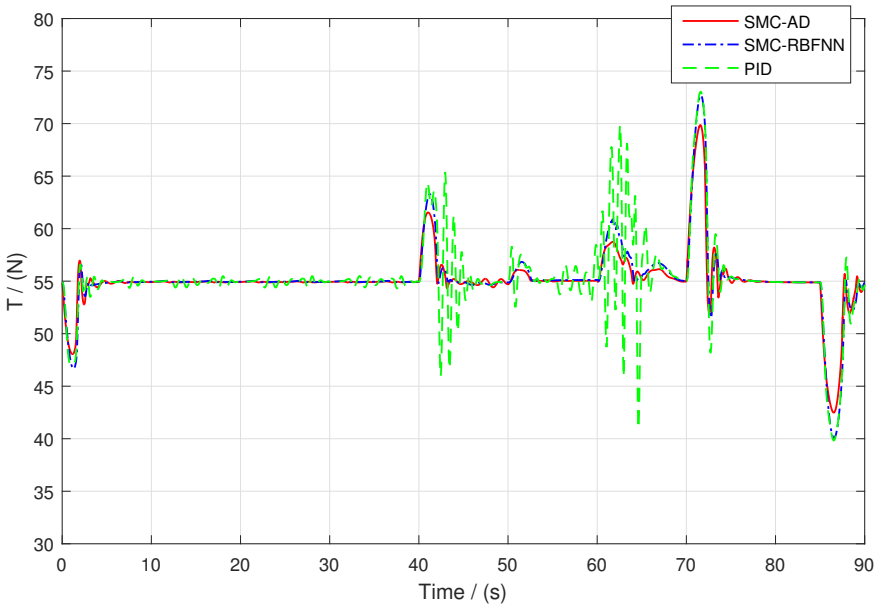

Figure 11. Virtual control thrust T.

Besides, the integral of absolute value of error (IAE) $IAE_x = \int_0^T |x| dt$ performance index is also used to compare the control performance of these three control schemes. The less value of the IAE index means faster convergence rate and better control performance. The IAE indexes acquired from the simulations are presented in Table 3. It can be observed that the indexes of the proposed SMC-AD control scheme in the position control are much smaller than the two other methods. As for the attitude control, the gap between the indexes of the proposed method and the other two methods are shorten. However, the performance of the SMC-AD control scheme is also better than the PID control and the

SMC-RBFNN control scheme. According to the results given above, it illustrates that the proposed method significantly improves the control performance of the tilt tri-rotor UAV in the hover mode.

Table 3. Integral of absolute value of error (IAE) indexes.

States	SMC-AD	SMC-RBFNN	PID
X	0.905	12.820	4.388
Y	1.227	8.260	6.885
Z	1.051	14.710	11.70
ϕ	0.542	1.656	1.253
θ	0.788	0.829	1.133
ψ	0.045	0.076	0.075

4.3. Experiment

In this subsection, an experiment is carried out on a tilt tri-rotor UAV designed by our lab to further verify the effectiveness of the proposed control scheme. The proposed cascade controller and control allocator are built in Pixhawk. To ensure flight safety, the aircraft is controlled manually, such that the desired position signal can be provided by the remote device. In the experiment, the tilt tri-rotor UAV first takes off vertically to a certain altitude. Then, the remote device adjusts the desired position signal, and the UAV flies to track the desired position signal. After the flight, it lands at the designated position. The experimental scene is shown in Figure 12.

Figure 12. Experimental scene of the tilt tri-rotor UAV in the hover mode.

The experiment results are shown in Figures 13–15. Figure 13 gives the position variations of the tilt tri-rotor UAV when it tracks the position signal given by remote control. The results show that the actual position curve is consistent with the desired position signal, which means that the proposed controller can guarantee good position tracking effect. In the proposed control scheme, the position control is achieved by the adjustment of the attitude, and the output of the position loop is the desired signal of the attitude loop. The tracking performance of the attitudes is shown in the Figure 14. In the flight process of the hover mode, the actual flight attitude can basically track the reference signal given by the position loop, but there will be a small tracking error. The pulse width modulation (PWM) inputs of the three motors are shown in the Figure 15. The experimental results show that the proposed control scheme in this paper has a good control effect on the position control and attitude control of the tilt tri-rotor UAV in the hover mode, and the application of this scheme will lay the foundation for the further control scheme design of the mode transition mode.

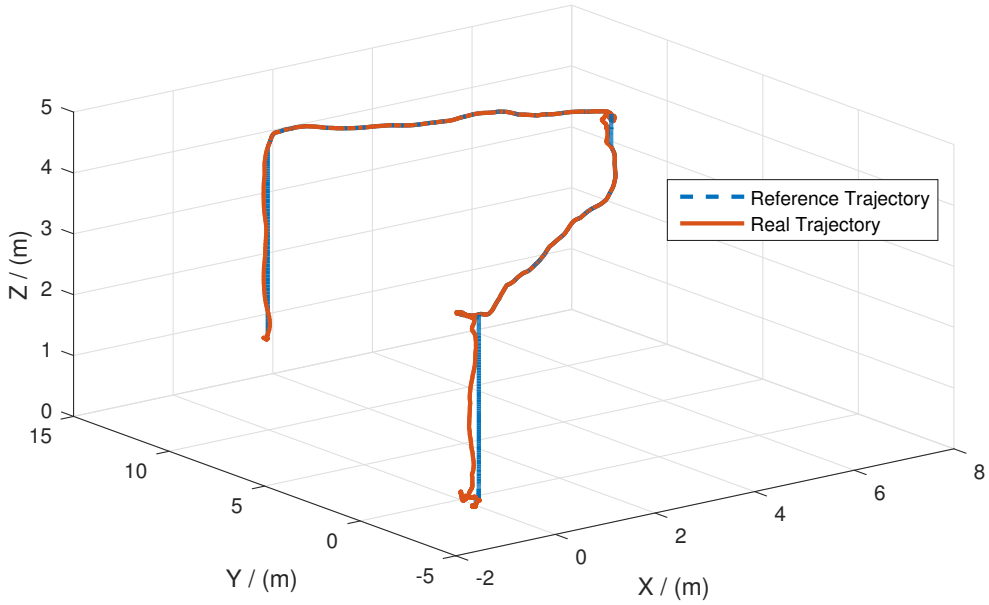

Figure 13. Position trajectories.

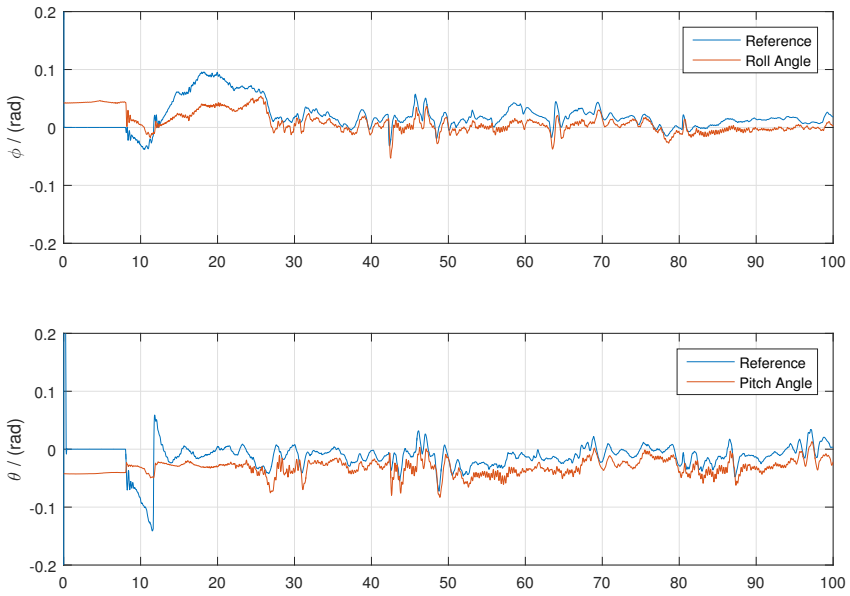

Figure 14. Attitude trajectories.

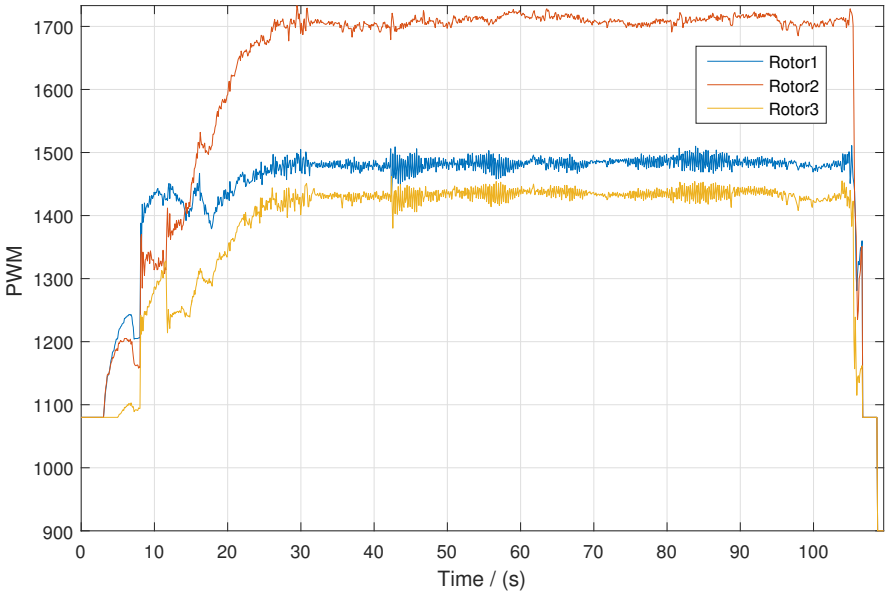

Figure 15. PWM value of the three rotors.

5. Conclusions

In this paper, a nonlinear robust sliding mode control approach based on auxiliary dynamic is proposed for the tilt tri-rotor UAV to achieve stable flight control in the hover mode. The model of the prototype is derived, and then a cascade controller consisting of position control and attitude control is developed. To improve the position control performance, SMC integral with the auxiliary dynamic system is proposed to provide reasonable constraints of the thrust and reference attitudes. SMC and disturbance observer are used to obtain strong robustness and high anti-interference ability in the attitude control. The proposed control scheme has been compared with PID control and SMC-RBFNN method, and the simulations show that the proposed control scheme has achieved better performance. The effectiveness of the whole control scheme is also verified by experiment. Future work will focus on the control scheme design of the transition mode of the tilt tri-rotor UAV.

Author Contributions: Conceptualization, G.H., L.Y., and X.W.; methodology, G.H., L.Y., and X.W.; software, L.Y. and H.H.; validation, G.H., L.Y., and H.H.; formal analysis, G.H. and L.Y.; investigation, G.H., L.Y., and H.H.; resources, X.W.; data curation, G.H. and H.H.; writing—original draft preparation, G.H. and L.Y.; funding acquisition, X.W. All authors have read and agreed to the published version of the manuscript.

Funding: This work is supported by the Natural Science Foundation of Hunan Province under grant 2019JJ50717, and in part by the National Natural Science Foundation of China under grant 61973309.

Conflicts of Interest: The authors declare no conflict of interest. The funders had no role in the design of the study; in the collection, analyses, or interpretation of data; in the writing of the manuscript; or in the decision to publish the results.

Appendix A

The control parameters of the proposed SMC-AD control scheme contain two parts: the parameters of the position loop and the parameters of the attitude loop. The parameters of the position loop are $k = 1, l = 1, k_\alpha = 1, k_\beta = 1$, $k_p = diag\{0.3 \quad 0.3 \quad 0.6\}$, $c_p = diag\{1.5 \quad 1.5 \quad 3\}, \varepsilon_p = 0.5$. The parameters of the attitude loop are $k_2 = diag\{10 \quad 10 \quad 2\}, k_a = diag\{4 \quad 4 \quad 1\}, c_a = diag\{2 \quad 2 \quad 1\}, \varepsilon_a = 0.2$.

The SMC-RBFNN control scheme also contain the position loop and the attitude loop. The parameters of the position loop are $k_p = 8, c_p = 12, \varepsilon_p = 0.1$. The parameters of the attitude loop

are $k_a = 0.1, c_a = 0.3, \varepsilon_a = 0.1$. The standard deviation of Gaussian function of the neural network is $\delta = [2.2 \quad 2.0 \quad 2.3]$. The mean value of Gaussian function(containing seven neurons) is

$$10^{-3} \begin{bmatrix} -1.5 & -1 & -0.5 & 0 & 0.5 & 1 & 1.5 \\ -1.5 & -1 & -0.5 & 0 & 0.5 & 1 & 1.5 \\ -1.5 & -1 & -0.5 & 0 & 0.5 & 1 & 1.5 \\ -1.5 & -1 & -0.5 & 0 & 0.5 & 1 & 1.5 \\ -1.5 & -1 & -0.5 & 0 & 0.5 & 1 & 1.5 \end{bmatrix}$$

The parameters of the PID control in the simulations are given in Table A1.

Table A1. The parameters of the PID control.

Controlled Channel	K_p	K_i	K_d
X	1	0.1	1
Y	0.5	0.05	0.5
Z	4	0.1	0.5
ϕ	10	1.8	0.1
θ	10	2	0
ψ	20	2	0

References

1. Liu, Z.; He, Y.; Yang, L.; Han, J. Control techniques of tilt rotor unmanned aerial vehicle systems: A review. *Chin. J. Aeronaut.* **2017**, *30*, 135–148. [CrossRef]
2. Bolkcom, C. *V-22 Osprey Tilt-Rotor Aircraft*; Congressional Research Service Reports; Library of Congress: Washington, DC, USA, 2005.
3. Lee, J.; Yoo, C.S.; Park, Y.S. An experimental study on time delay control of actuation system of tilt rotor unmanned aerial vehicle. *Mechatronics* **2012**, *22*, 184–194. [CrossRef]
4. Kang, Y.; Kim, N.; Kim, B.S.; Tahk, M.J. Autonomous waypoint guidance for tilt-rotor unmanned aerial vehicle that has nacelle-fixed auxiliary wings. *Pap. Present. Inst. Mech. Eng. Part J. Aerosp. Eng.* **2014**, *228*, 2695–2717. [CrossRef]
5. Zivan, L.; Wolff, A.; Dekel, G.; Efraty, Y. IAI Mini Panther-an Innovative VTOL UAV design. In Proceedings of the 54th Israel Annual Conference on Aerospace Sciences, Haifa, Israel, 19–20 February 2014; pp. 1688–1701.
6. Aktas, Y.O.; Ozdemir, U.; Dereli, Y.; Tarhan, A.F.; Cetin, A.; Vuruskan, A.; Yuksek, B.; Cengiz, H.; Basdemir, S.; Ucar, M.; et al. Rapid prototyping of a fixed-wing VTOL UAV for design testing. *J. Intell. Robot. Syst.* **2016**, *84*, 639–664. [CrossRef]
7. Roman, C.; Marcin, L.; Zbigniew, G.; Tomasz, K. Construction Prototyping, flight dynamics modeling, and aerodynamic analysis of hybrid VTOL unmanned aircraft. *J. Adv. Transp.* **2018**, *74*, 371–393. [CrossRef]
8. Ozdemir, U.; Aktas, Y.O.; Vuruskan, A.; Dereli, Y.; Tarhan, A.F.; Demirbag, K.; Erdem, A.; Kalaycioglu, G.D.; Ozkol, I.; Inalhan, G. Design of a commercial hybrid VTOL UAV system. *J. Intell. Robot. Syst.* **2014**, *74*, 371–393. [CrossRef]
9. Yuksek, B.; Vuruskan, A.; Ozdemir, U.; Yukselen, M.A.; Inalhan, G. Transition flight modeling of a fixed-wing vtol uav. *J. Intell. Robot. Syst.* **2016**, *84*, 83–105. [CrossRef]
10. Papachristos, C.; Alexis, K.; Tzes, A. Model predictive hovering-translation control of an unmanned tri-tiltrotor. In Proceedings of the 2013 IEEE International Conference on Robotics and Automation (ICRA), Karlsruhe, Germany, 6–10 May 2013; pp. 5425–5432. [CrossRef]
11. Kostas, A.; Papachristos, C.; Siegwart, R.; Anthony, T. Robust model predictive flight control of unmanned rotorcrafts. *J. Intell. Robot. Syst.* **2016**, *81*, 443–469. [CrossRef]
12. Chen, Z.B.; Jia, H.G. Design of flight control system for a novel tilt-rotor UAV. *Complexity* **2020**, 4757381. [CrossRef]

13. Carlson, S. A hybrid tricopter/flying-wing vtol uav. In Proceedings of the 52nd Aerospace Sciences Meeting, National Harbor, MD, USA, 13–17 January 2014. [CrossRef]
14. Chowdhury, A.B.; Kulhare, A.; Raina, G. A generalized control method for a Tilt-rotor UAV stabilization. In Proceedings of the 2012 IEEE International Conference on Cyber Technology in Automation, Control, and Intelligent Systems, Bangkok, Thailand, 27–31 May 2012; pp. 309–314. [CrossRef]
15. Xian, B.; Hao, W. Nonlinear Robust Fault-Tolerant Control of the Tilt Trirotor UAV Under Rear Servo's Stuck Fault: Theory and Experiments. *IEEE Trans. Ind. Inform.* **2019**, *15*, 2158–2166. [CrossRef]
16. Sergio, G.N.; Jesus, V.C.; Federico, P.V.; Jose, V.S.; Raul, S. Motion Equations and Attitude Control in the Vertical Flight of a VTOL Bi-Rotor UAV. *Electronics* **2019**, *208*, 208. [CrossRef]
17. Govdeli, Y.; Muzaffar, S.M.; Raj, R.; Elhadidi, B.; Kayacan, E. Unsteady aerodynamic modeling and control of pusher and tilt-rotor quadplane configurations. *Aerosp. Sci. Technol.* **2019**, *94*, 105421. [CrossRef]
18. Liu, N.J.; Cai, Z.H.; Zhao, J.; Wang, Y.X. Predictor-based model reference adaptive roll and yaw control of a quad-tiltrotor UAV. *Chin. J. Aeronaut.* **2020**,*33*, 282–295. [CrossRef]
19. Francesco, G.; Mattei, M.; Amato, E.D. Incremental nonlinear dynamic inversion and control allocation for a tilt rotor UAV. In Proceedings of the AIAA Guidance, Navigation, and Control Conference, National Harbor, MD, USA, 13–17 January 2014; p. 0963. [CrossRef]
20. Kong, Z.; Lu, Q. Mathematical Modeling and Modal Switching Control of a Novel Tiltrotor UAV. *J. Robot.* **2018**, *2018*, 1–12. [CrossRef]
21. Yildiz, Y.; Unel, M.; Demirel, A.E. Adaptive nonlinear hierarchical control of a quad tilt-wing UAV. In Proceedings of the 2015 European Control Conference (ECC), Linz, Austria, 15–17 July 2015; pp. 3623–3628. [CrossRef]
22. Papachristos, C.; Alexis, K.; Tzes, A. Dual–authority thrust–vectoring of a tri-tiltrotor employing model predictive control. *J. Intell. Robot. Syst.* **2016**, *81*, 471–504. [CrossRef]
23. Yoo, C.S.; Ryu, S.D.; Park, B.J.; Kang, Y.S.; Jung, S.B. Actuator controller based on fuzzy sliding mode control of tilt rotor unmanned aerial vehicle. *Int. J. Control. Autom. Syst.* **2014**, *12*, 1257–1265. [CrossRef]
24. Yin, Y.C.; Niu, H.W.; Liu, X.B. Adaptive neural network sliding mode control for quad tilt rotor aircraft. *Complexity* **2017**, *2017*, 1–13. [CrossRef]
25. Yang, Y.N.; Yan, Y. Neural network approximation-based nonsingular terminal sliding mode control for trajectory tracking of robotic airships. *Aerosp. Sci. Technol.* **2016**, *54*, 192–197. [CrossRef]
26. Fu, J.; Wu, Q.X.; Chen, W.H.; Yan, X.G. Chattering-free condition for sliding mode control with unidirectional auxiliary surfaces. *Trans. Inst. Meas. Control.* **2013**, *35*, 593–605. [CrossRef]
27. Li, S.; Wang, Y.; Tan, J. Adaptive and robust control of quadrotor aircrafts with input saturation. *Nonlinear Dyn.* **2017**, *89*, 255–265. [CrossRef]
28. Zhu, B.; Huo, W. Nonlinear control for a model-scaled helicopter with constraints on rotor thrust and fuselage attitude. *Acta Autom. Sin.* **2014**, *40*, 2654–2664. [CrossRef]
29. Sun, J.L.; Liu, C.S. Auxiliary-system-based composite adaptive optimal backstepping control for uncertain nonlinear guidance systems with input constraints. *ISA Trans.* **2020**. [CrossRef] [PubMed]
30. Cetinsoy, E.; Dikyar, S.; Hançer, C.; Oner, K.T.; Sirimoglu, E.; Unel, M.; Aksit, M.F. Design and construction of a novel quad tilt-wing UAV. *Mechatronics* **2012**, *22*, 723–745. [CrossRef]
31. Vladislav, K.; Eugene, A. *Aircraft System Identification: Theory and Practice*; American Institute of Aeronautics and Astronautics: Reston, VA, USA, 2006.
32. Yu, L.; He, G.; Zhao, S.L.; Wang, X.K.; Shen, L.C. Immersion and Invariance-based Sliding Mode Attitude Control of Tilt Tri-rotor UAV in Helicopter Mode. *Int. J. Control. Autom. Syst.* **2020**, in press.
33. Zhao, B.; Xian, B.; Zhang, Y.; Zhang, X. Nonlinear robust sliding mode control of a quadrotor unmanned aerial vehicle based on immersion and invariance method. *Int. J. Robust Nonlinear Control.* **2016**, *25*, 3714–3731. [CrossRef]
34. Hu, J.; Zhang, H.; Subbarao, K. Immersion and invariance based command-filtered adaptive backstepping control of VTOL vehicles. *Automatica* **2013**, *49*, 2160–2167. [CrossRef]
35. Bertsekas, D.P. *Nonlinear Programming*; Athena Scientific: Belmont, TN, USA, 1999.

36. An C.; Zhang, D.; Zhang, J.; Li, T. A New structural configuration of tilting rotor unmanned aerial vehicle modeling. In Proceedings of the 35th Chinese Control Conference, Chengdu, China, 27–29 July 2016; pp. 2120–2125. [CrossRef]
37. Yu, L.; He, G.; Zhao, S.L.; Wang, X.K. Dynamic inversion-based sliding mode control of a tilt tri-rotor UAV. In Proceedings of the 12th Asian Control Conference, Fukuoka, Japan, 9–12 June 2019; pp. 1637–1642.